Temporal Change in Near-source Attenuation Probably due to the Pore Pressure Diffusion in the Source Region of the Intense Earthquake Swarm in the Yamagata-Fukushima border, NE Japan

Keisuke Yoshida[1]

[1]Tohoku University

Corresponding author: Keisuke Yoshida, Research Center for Prediction of Earthquakes and Volcanic Eruptions, Tohoku University, 6-6 Aza-Aoba, Aramaki, Aoba-ku, Sendai, 980-8578, Japan. (keisuke.yoshida.d7@tohoku.ac.jp)

Key Points:

- Seismic attenuation near earthquake sources were estimated by a novel approach for an intense swarm caused by the 2011 Tohoku-Oki earthquake
- Estimated near-source attenuation is higher near the fault zone than in the surrounding area especially in the initial period of the swarm
- Near-source attenuation changes with time with other source and seismicity characteristics reflecting the pore pressure change

Abstract

Existence of fluids in the crust is key to understanding the occurrence of earthquakes because it affects the fault strength. Given that fluids are intensely distributed in fault zones, anelastic attenuation of seismic waves may be locally high in these regions. The present study examined near-source attenuation in the focal region of the intense swarm activity in the Yamagata-Fukushima border region of Japan by a new simple approach. This earthquake swarm exhibits a distinctive migration behavior of hypocenters similar to fluid-injection induced seismicity and was estimated to be caused by the pore pressure change. Near-source attenuation was estimated by examining the decay of amplitude ratios of nearby earthquake pairs with travel time differences. The obtained $\boldsymbol{Q^{-1}}$ was high during the initial ~50 days (with a median value of 0.040 for 2-4 Hz), and significantly decreased to become almost constant for the later period (with a median value of 0.011). This pattern is similar to those independently obtained for background seismicity rate, b-value, stress drop, and fault strength. These patterns can be explained in a consistent manner by the hypothesis that the swarm in question was triggered by fluid movement following the 2011 Tohoku-Oki earthquake, and the source and seismicity characteristics were also affected by this temporal change in pore pressure. Attenuation was high near the earthquake sources than that in the surrounding crust in the initial period of the swarm, indicating the importance of considering the near-source attenuation to correctly estimate the source-effect of an earthquake.

Plain Language Summary

Fluid movements inside the Earth largely affects the occurrence of earthquakes by modulating the fault strength. Seismic waveforms provide information about anelastic properties of rocks via the attenuation of waveform amplitude, which is an important clue to the presence of fluids. The spatial resolution of anelastic property, however, is generally insufficient to resolve whether the fluids intensely distribute near the fault zone or not. The present study examined the anelastic properties near earthquake hypocenters by a novel approach. The target earthquake sequence is a large earthquake swarm in the crust of Japan, which was estimated to be caused by the fluid movements after the 2011 M9 Tohoku-Oki earthquake. The results indicate that the intensity of seismic attenuation is higher near the fault zone than in the surrounding area. Moreover, the intensity of seismic attenuation changed with time synchronously with other earthquake and seismicity characteristics. The synchronous temporal changes can be explained by presuming that fluids are intensely distributed in the focal region of the swarm, and it diffused with time with affecting earthquake occurrence. The results indicate the importance of monitoring the fluid behavior at depth to understand the occurrence and characteristics of earthquakes.

1 Introduction

Increases in pore pressure decrease the fault strength, and thus may play an important role in the occurrence of earthquakes (e.g., Hasegawa et al., 2005; Hubbert and Rubey, 1959; Nur and Booker, 1972; Sibson, 1992). One may consider a possibility that the seismogenic zone has a larger amount of fluids than in the surrounding crust. Given that fluids are intensely distributed in fault zones, anelastic attenuation of seismic waves may be locally high in these regions (e.g., Winkler & Nur, 1982). The spatiotemporal variation of the seismic attenuation structure provides information about the states of fault zones including the presence of fluids and the fault damage (e.g., Hauksson & Shearer, 2006).

Previous studies have investigated the attenuation structure on a regional scale in many global locations, summarized by Sato et al. (2012). However, only few studies (e.g., Matsumoto et al., 2009; Kriegerowski et al., 2019) have attempted to directly estimate the attenuation structure near the earthquake source (hereafter, referred to as “near-source attenuation”). As an exception, Matsumoto et al. (2009) proposed a method for estimating the attenuation structure in a seismically active region based on the spectral ratios of two earthquakes. They used coda waves to remove the source-effects, computed spectral ratios at many different stations, and estimated the spatial variation of attenuation structure in the aftershock area of the 2005 M7.0 West Off Fukuoka Prefecture Earthquake. Kriegerowski et al. (2019) developed another method using the spectral ratios of two earthquakes with some additional assumptions. The assumptions include that the attenuation structure is constant over the analyzed frequency range and the source spectra completely follow the ω^2-model (Aki, 1967). Their method may give an estimate of the attenuation structure even from a single seismic station owing to the additional assumptions. However, many of their results have unphysical negative values of the attenuation factor, which might come from the error of above assumptions. The present study developed a simple method with fewer assumptions than the previous works to estimate the near-source attenuation.

A possible way to directly estimate the near-source attenuation is to examine the decay of amplitude ratios of two nearby earthquakes with travel time differences (Fig. 1a). Such an analysis is usually not easy because it requires precisely-measured arrival time difference and amplitude ratio data from various seismic stations. The present study overcame the problem by using the waveform correlation technique (Poupinet et al., 1984) to precisely measure the differential arrival time and amplitude ratio data. Also, source-effects first need to be removed from the recorded waveform data. The present study analyzed dataset satisfying the following two conditions: (1) the analyzed frequency range is sufficiently lower than the source corner frequencies and (2) the focal mechanisms of the two earthquakes are similar. Note that even a frequency range higher than the corner frequency might be available if the spectral falloffs are the same between the two events (such as the ω^2-model), and the corner frequencies are the same among the different seismic stations for the earthquake pair. However, such an assumption does not hold for even a simple physical source model (Kaneko & Shearer, 2014). Therefore, the present study only used the frequency range less than the source corner frequency.

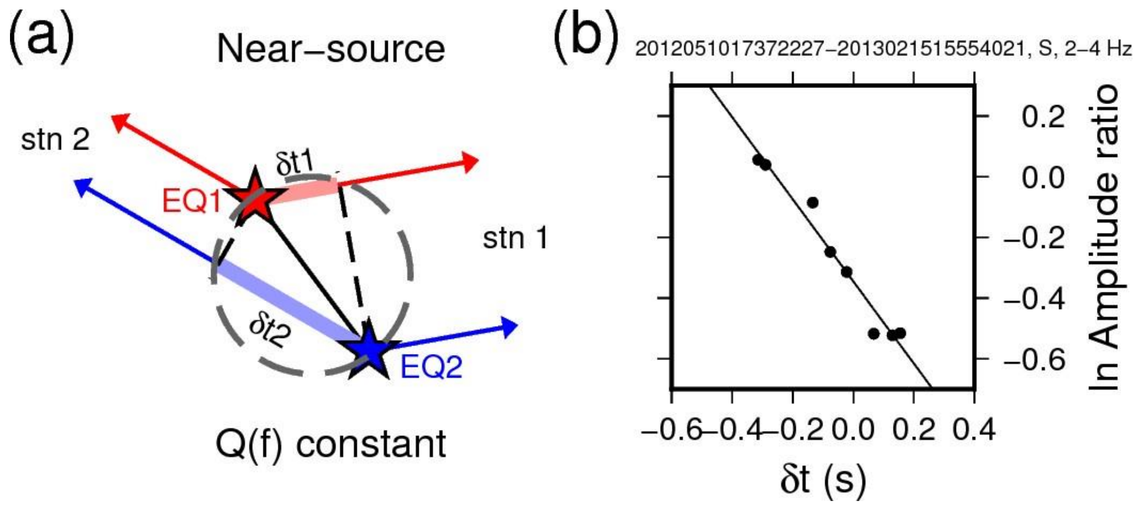

Figure 1. (a) A schematic illustration of the principle of estimating near-source attenuation. (b) An example of the relationship between amplitude ratios, $A_{1\mathrm{i}}(f)/A_{2\mathrm{i}}(f)$, and differential arrival times, δt_{i}, of an earthquake pair.

The present study developed a method using the similarity of waveforms of nearby earthquakes to precisely derive the amplitude ratios and the travel time differences. The method was applied to the intense swarm activity in the crust of the Yamagata-Fukushima border region of Japan (Fig. 2a). Many earthquakes with similar focal mechanisms occurred in a small part of this source region (Yoshida et al., 2016, 2019a and 2019b; Yoshida & Hasegawa, 2018). The similarity of the waveforms in the source region supplies precise differential arrival time and amplitude ratio data by using waveform cross-correlation (Yoshida & Hasegawa, 2018). The focal area is surrounded by the Japanese national dense seismic network. This network enables the examination of near-source attenuation in the region.

Previous studies suggest that the Yamagata-Fukushima border swarm has been triggered by fluid movement following the 2011 Tohoku-Oki earthquake (Terakawa et al., 2013; Yoshida et al., 2016, 2019a). In fact, the swarm activity began despite a reduction in shear stress after the 2011 Tohoku-Oki earthquake, with a delay of six days. Hypocenters show a distinct migration behavior, which is similar to fluid-injection-induced seismicity (e.g., Shapiro et al., 1997), from deeper to shallower levels along several planar structures (Yoshida & Hasegawa, 2018). Previous studies have reported the temporal variations in the hypocenters (Okada et al., 2015; Yoshida & Hasegawa, 2018), fault strength (Yoshida et al., 2016), stress drop (Yoshida et al., 2017, 2019b), b-values (Yoshida et al., 2017), and background seismicity rate (Yoshida & Hasegawa, 2018) in the source region of the swarm (Figs. 2b), which have been interpreted as resulting from temporal changes in fault strength due to pore pressure diffusion. As such, comparing the temporal changes in near-source attenuation with these source- and seismicity- parameters is of great interest.

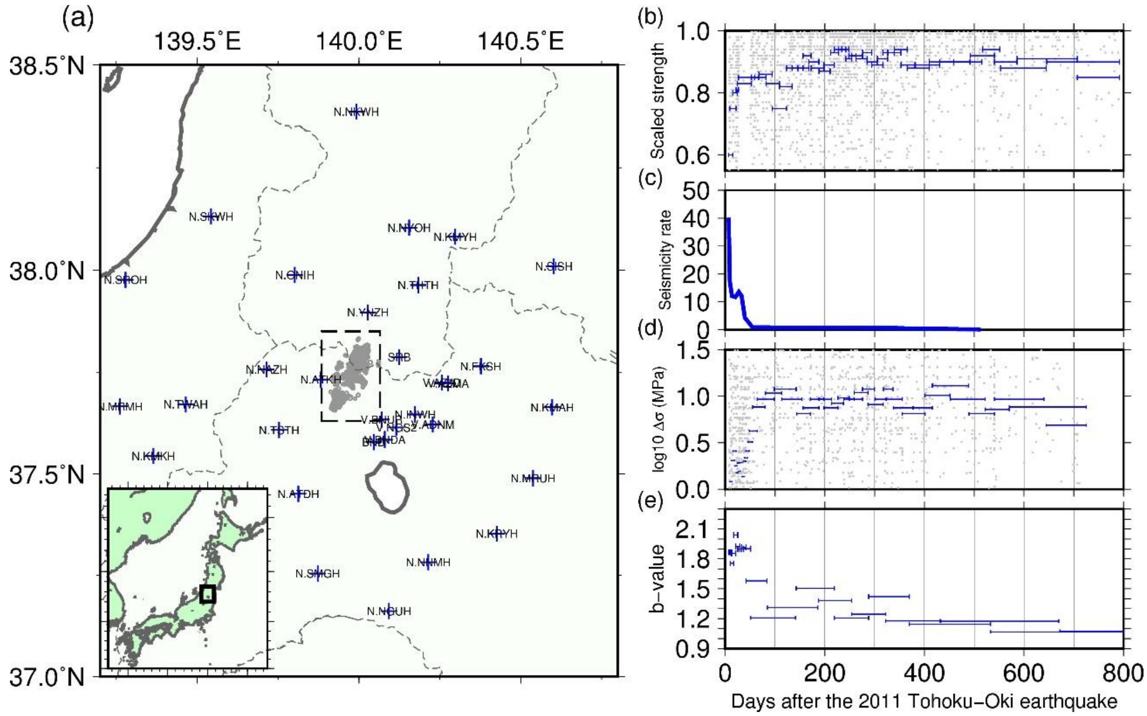

Figure 2. (a) Distribution of hypocenters (gray circles) and seismic stations (blue crosses) in the study area. The range is shown by the bold rectangle in the insert map. (b), (c), (d) and (e): Temporal variations in fault strength (Yoshida et al., 2016), background seismicity rate (Yoshida & Hasegawa, 2018), stress drop (Yoshida et al., 2019b), and b-value (Yoshida et al., 2017), respectively. In (b) and (d), individual results and geometric means are shown by gray circles and blue lines, respectively.

2 Data and Method

The amplitude attenuation due to anelastic attenuation can be described by the seismic quality factor $Q = -\frac{2\pi E}{\Delta E}$, where E is the energy of a seismic wave and ΔE is the energy lost during one cycle. In seismology, amplitude attenuation over elapsed time is related to Q^{-1} by the following approximation ($Q \gg 1$):

$$\ln(r^{\gamma} A_i(f)) = -\pi f Q^{-1}(f) t + \text{Constant} \quad (1)$$

where f is frequency, r is distance from the source, γ is the exponent of the geometric spreading factor depending on the ray-path, and t is elapsed time. Here Q^{-1} is the combination of amplitude attenuations due to both intrinsic and scattering losses. The Q^{-1} values above ~1 Hz range from 10^{-4} to 10^{-1} in many regions of the world and decrease with frequency (Sato et al., 2012).

To estimate the near-source attenuation, the relationship between the amplitude ratios $A_{1\mathrm{i}}/A_{2\mathrm{i}}$ and the relative travel times $\delta t_{\mathrm{i}} = t_{1\mathrm{i}} - t_{2\mathrm{i}}$ from two nearby (~ 1 km) earthquakes were used (Fig. 1a). Here, $A_{1\mathrm{i}}$ and $A_{2\mathrm{i}}$ are the amplitudes, and $t_{1\mathrm{i}}$ and $t_{2\mathrm{i}}$ are the travel times for the two events (event-1 and event-2, respectively) at the *i*th-station. By assuming the same site- and propagation-effects along the common path of the two nearby earthquakes,

$$\ln\frac{A_{1i}(f)}{A_{2i}(f)} = -\pi f Q^{-1}(f)\delta t_{\mathrm{i}} + \mathrm{Constant} \quad (2)$$

Here, the effect of geometrical spreading was ignored because the distance between the two earthquakes is much smaller than the distance between the earthquakes and the stations. Eq. (2) shows that $Q^{-1}(f)$ near the source can be estimated by precisely measuring the amplitude ratios, $A_{1\mathrm{i}}(f)/A_{2\mathrm{i}}(f)$, and the travel time differences, δt_{i} , at various stations. This concept is similar to that of Lin & Shearer (2007) for estimating the near-source Vp/Vs by using the ratios of precisely measured differential arrival times of P- and S-waves. Although the method of Lin & Shearer (2007) needs to assume that the ray paths of P- and S-waves is the same, the present method to determine Q^{-1} does not need the assumption. The present method is also similar to the method proposed by Matsumoto et al. (2009) for estimating the Q^{-1}-value in the fault zone. However, the present method is focused on the near-source attenuation and only uses the low frequency range. The present method is much simpler and robust for modeling errors because it does not need to model or cancel out the source effects.

Fig.1 (a) shows the distribution of earthquake hypocenters and seismic stations. The seismic network is composed of seismic stations of Tohoku University, NIED Hi-net, and V-net. The waveform data is available at the website of NIED Hi-net (http://www.hinet.bosai.go.jp/?LANG=en). In the period from March 11, 2011 to 2016, 2,347 M 2-3 earthquakes were used from the JMA unified catalog (https://www.data.jma.go.jp/svd/eqev/data/bulletin/hypo_e.html).

Analyzed earthquake pairs needed to have similar focal mechanisms, which were confirmed by previous studies (Yoshida et al., 2016, 2019b). I first assumed that the difference of focal mechanism does not affect the estimation of near-source Q^{-1}, and checked the assumption in detail in the Discussion section. In the following analyses, I only used earthquake pairs with cross-correlation coefficients >0.85 both for P- and S-waves from at least eight different stations. The length of the time-window was set to 2.0 s, and the time-window began 0.3s before the arrival times. The arrival times were derived from the JMA unified catalog or theoretically estimated based on the origin time and the hypocenter, based on the 1-D velocity structure model JMA2001 (Ueno et al., 2002). Both the transverse and radial components of the S-waves were used for estimating Q^{-1} because of the high S/N ratio.

The frequency range was set to 2-4 Hz, which is sufficiently lower than the source corner frequencies of the M2-3 earthquake S-waves (Yoshida et al., 2017). The central frequency (3 Hz) was used as f in eq. (2). The results from other frequency ranges of the S-waves and those of the P-waves are compared to the main result in the Discussion section.

Differential arrival times were precisely measured by waveform cross-correlation. Since the frequency ranges are narrow, amplitude ratios were measured in the time-domain using a principal component fit of aligned waveforms at each time, based on the waveform cross-correlation (Shelly et al., 2016). Data with low cross-correlation coefficients (cc<0.8) were discarded.

Fig. 1 (b) shows an example of comparing the amplitude ratios, $A_{1\mathrm{i}}(f)/A_{2\mathrm{i}}(f)$, with the travel time differences, δt_{i}, for an earthquake pair. The decreasing trend of $A_{1\mathrm{i}}(f)/A_{2\mathrm{i}}(f)$ with δt_{i} is clearly visible. Other examples are shown in Fig 3. The slope was measured using the least squares method by minimizing the difference between observed and predicted $\ln A_{1\mathrm{i}}(f)/A_{2\mathrm{i}}(f)$, which determines Q^{-1} from Eq. (2). We here assumed that the measurement error of δt is much smaller than $\frac{A_{1\mathrm{i}}(f)}{A_{2\mathrm{i}}(f)}$.

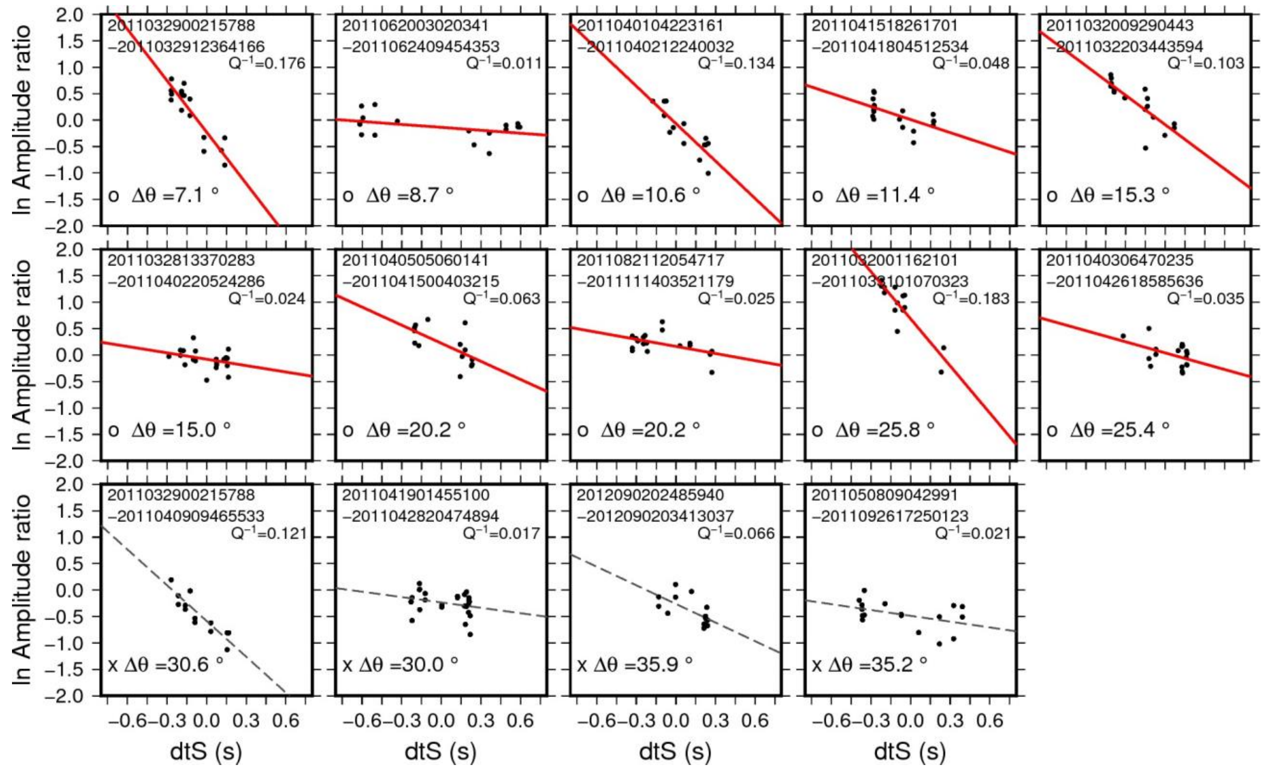

Figure 3. Examples of the determination of Q^{-1}-values.

To avoid solutions largely affected by outliers, 2000 estimations based on bootstrap re-sampling were performed, and the median value was used as the best result. The results of the bootstrap re-sampling were also used to evaluate the estimation error. Finally, 1,893 of 13,514 measurements were obtained by discarding any results that satisfied any of the following conditions: (1) the uncertainty error in the slope ($\Delta\theta$) was large ($> 30°$ in the 95% confidence interval), (2) the number of data used were less than 12, or (3) the difference between the maximum and minimum values of δt was less than 0.4 s. Fig. 4 (a) shows the frequency distribution of distances of earthquake pairs for which the near-source attenuation was obtained. The locations of hypocenters were taken from Yoshida & Hasegawa (2018) who relocated hypocenters precisely by using the waveform correlation. The mean and median distances are 1.1 and 1.2 km, respectively, and most of earthquake pairs are closer than 2 km.

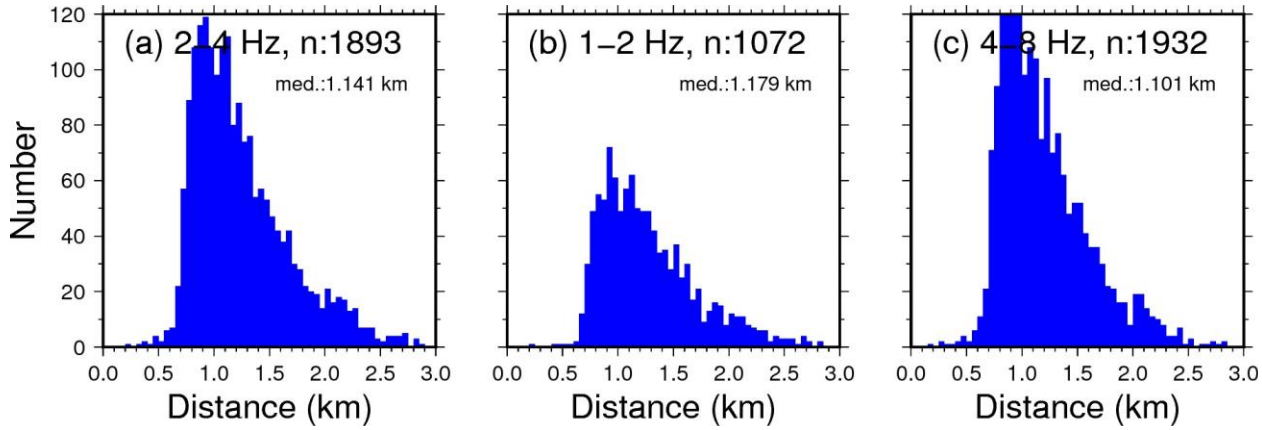

Figure 4. Frequency distributions of distances of earthquake-pairs used for the determination of Q^{-1}-values. (a) 2-4 Hz, (b) 1-2 Hz, (c) 4-8 Hz.

3 Results

Fig. 5 (a) shows the frequency distribution of obtained Q^{-1}-values. Negative values were sometimes estimated when the amplitude decay was not clear, although obtained values are positive for most cases (positive for 1200 of 1893 results). Since individual estimates are scattered, hereafter characteristics of obtained Q^{-1}-values were only statistically examined without discarding results with negative values. The median value was 0.011, and the 95 % uncertainty range, based on the bootstrap re-sampling of 2000 simulated dataset, was 0.010-0.013. These values were comparable to the regional values of ~0.01 around the source region estimated using the coda normalization method (Yoshida et al., 2017). This suggests that attenuation is not especially stronger near the fault zone of this swarm activity than in the surrounding regions as a whole.

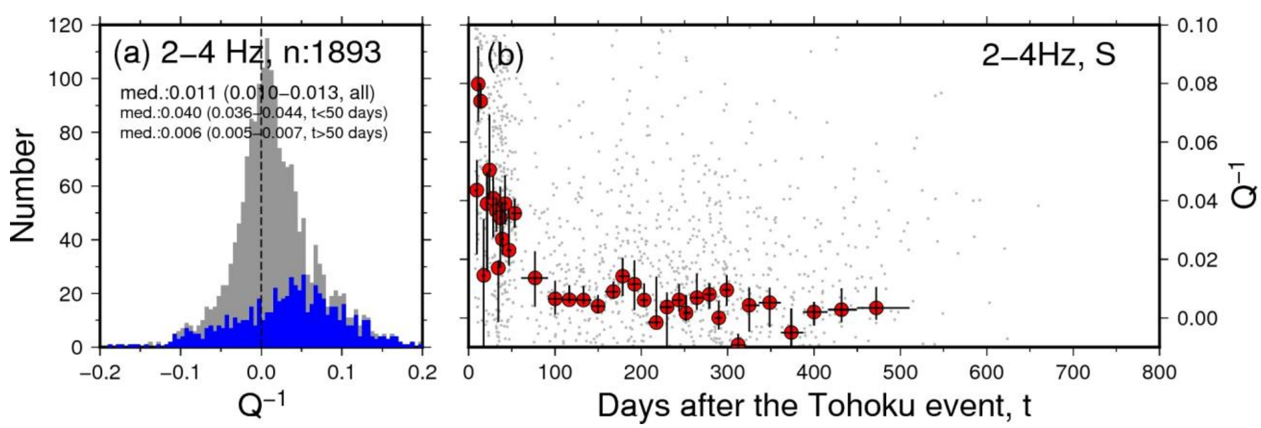

Figure 5. Results of near-source attenuation analyses. (a) Frequency distribution of obtained near-source Q^{-1}-values. Gray shows the result for all the analyzed periods. Blue shows the results for up to 50 days after the 2011 Tohoku-Oki earthquake. (b) Temporal changes in the

near-source Q^{-1}-values. Gray circles show individual results and red circles show median values of 30 bins having the same number of results. Vertical line indicates the 95% confidential interval based on 2000 bootstrap re-samplings.

To see the spatial variation of Q^{-1}, I computed mean values of Q^{-1} at evenly spaced 200x200x200 points which divides the entire region in latitude (37.63-37.85°), longitude (139.885-140.045°), and depth (4.0-14.0 km). I assumed that the obtained Q^{-1}-value basically represents an average value within the sphere whose diameter is the distance of the two earthquakes and whose center is the mean location (Fig. 1a). I used relocated hypocenters by Yoshida & Hasegawa (2018) for the locations of earthquake-pairs, and allocated Q^{-1}-values to all the points within the sphere. The mean values were obtained at the point only when the number was greater than or equal to 5.

The spatial variation of Q^{-1} thus obtained is shown in Figs. 6 (a)-(d) at the depths of 7.2, 7.8, 8.4 and 9.0 km in map-views and Fig. 7 in cross-sectional views. They tend to be high in the central part of the focal region. Locations of hypocenters in the initial stage shown in Figs. 6 (e)-(f) highlighted by red color appears to correspond to the locations with high Q^{-1}-value. Previous studies suggest that earthquakes in the initial period of this swarm have abnormally low stress drops (Yoshida et al., 2017, 2019b), high b-values (Yoshida et al., 2017), and high background seismicity rates (Yoshida & Hasegawa, 2018) compared to the later period (Fig. 2b-e). These changes were estimated to reflect the diffusion of pore pressure; especially high pore pressure in the initial stage and its temporal decrease (Yoshida et al., 2017). These suggest a possibility that the spatial variation of Q^{-1} in Figs. 6 (a)-(d) actually reflects the temporal variation due to the pore pressure diffusion.

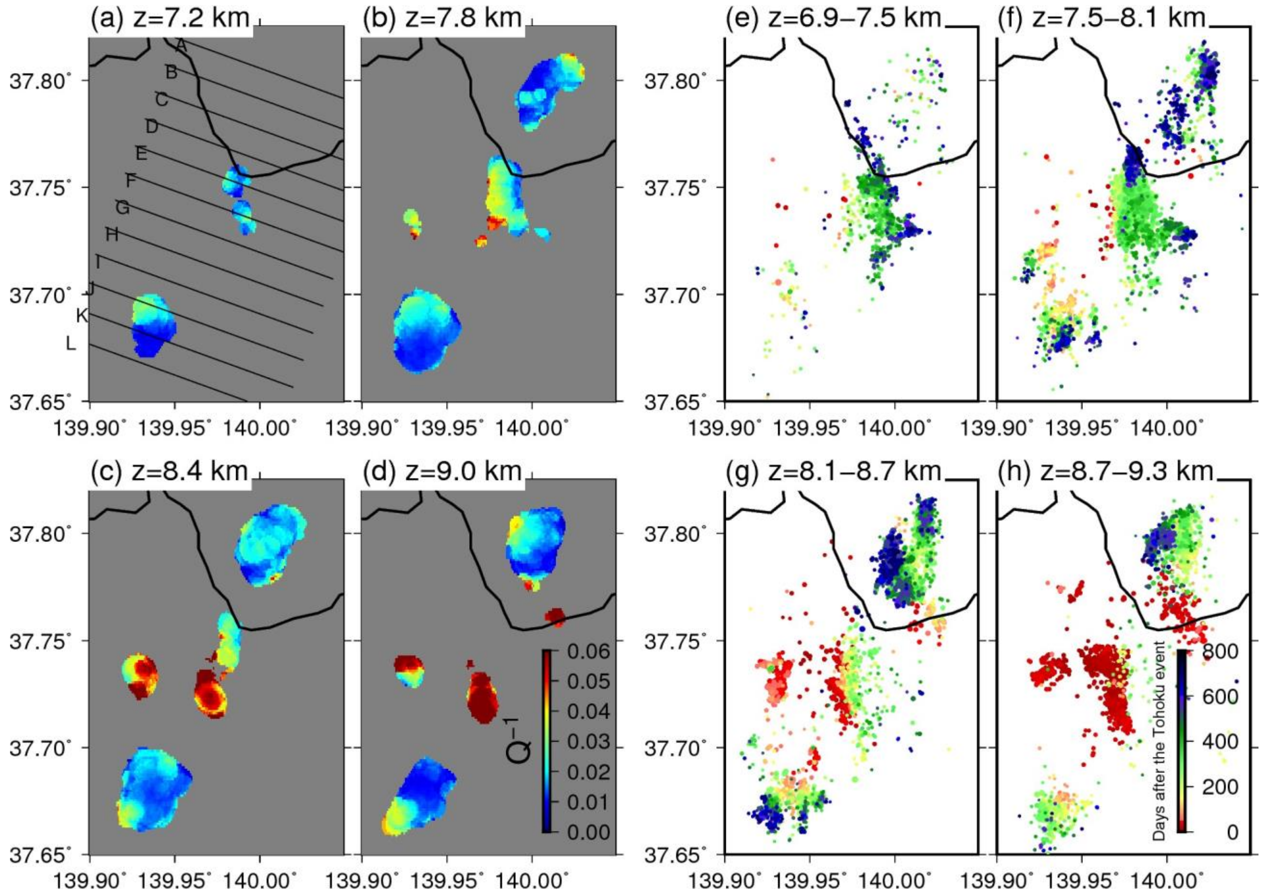

Fig. 6. (a)-(d) Spatial distribution of Q^{-1} for the 2-4 Hz frequency range at the different four depths. Q^{-1} values are shown by the color scale. (e)-(f) Spatial distribution of hypocenters determined by Yoshida & Hasegawa (2018). Occurrence timings were shown by the color scale.

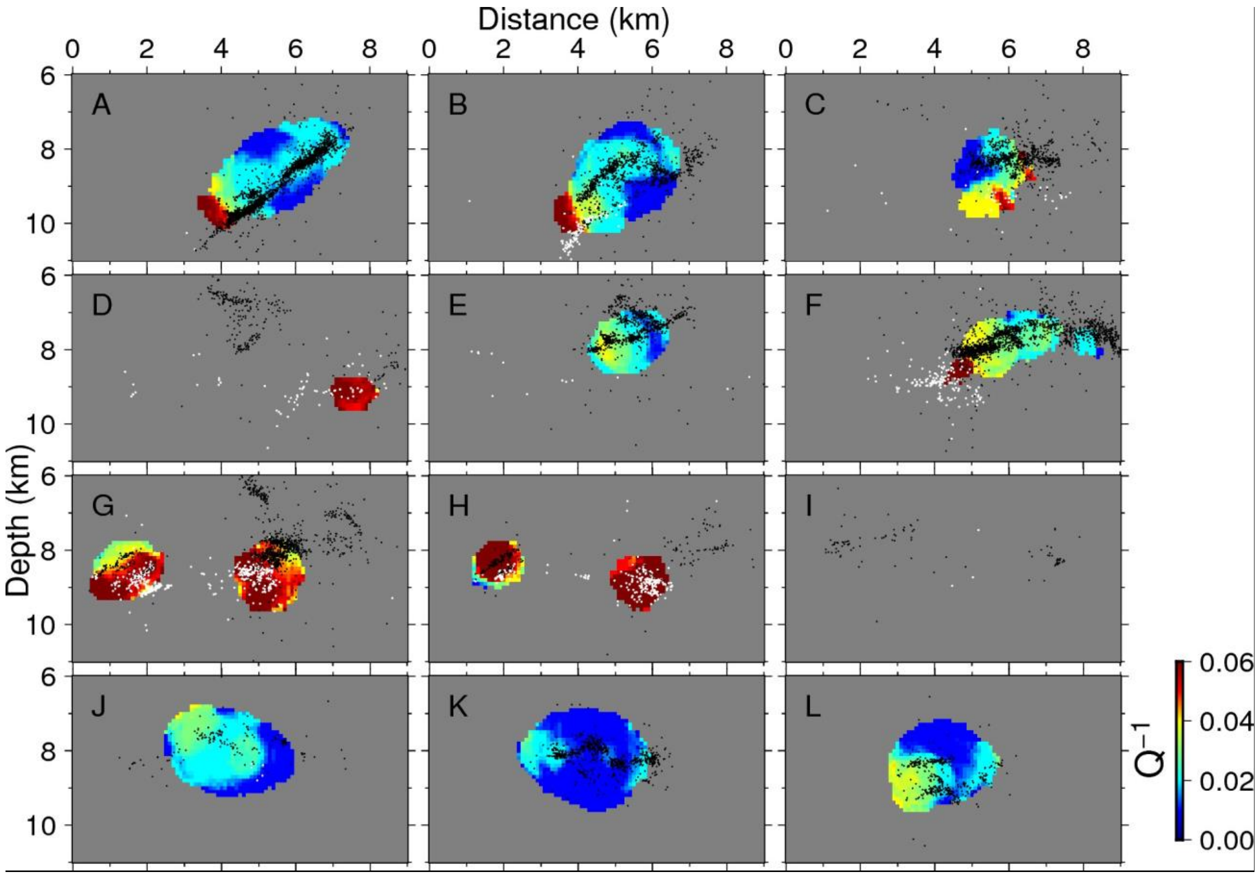

Fig. 7. Cross-sectional views of Q^{-1} for the frequency range of 2-4 Hz along the lines shown in Fig. 6 (a). Q^{-1} values are shown by the color scale. White and black circles show hypocenters in the initial 50 days and the later period, respectively.

Fig. 5 (b) compares Q^{-1} with occurrence time, which is the mean value for the earthquake pairs. The values vary over a wide range, but their median value exhibits a characteristic temporal variation. Q^{-1} values were high for the initial ~50 days (with a median value of 0.040 and a 95 % confidence interval of 0.036-0.044), and they decreased and became almost constant in the later period (with a median value of 0.006 and a 95 % confidence interval of 0.005-0.007). Although the Q^{-1} values for the later period are not very different from the regional value of ~ 0.01, the Q^{-1} values for the initial period are much higher than the regional value. Fig. 5 (b) includes results determined by earthquake pairs with a large time interval. The temporal pattern does not largely alter if only results with a relatively short time interval (< 30 days) are used (Fig. S1).

The temporal pattern of Q^{-1} values appears to be correlated with those of source- and seismicity-parameters, including fault strength, background seismicity rate, stress drop, and b-value (Figs. 2b-e), which were estimated independently. Fault strength and stress drop were low in the initial period (~ 50 days after the earthquake) and then increased to be almost constant in the later period (Figs. 2b and d). Seismicity rate and b-value were high in the initial period and then decreased to be almost constant in the later period (Figs 2c and e). Their values were abnormal during the initial period, and changed to almost constant typical values. This tendency is similar to the temporal change in Q^{-1} values obtained in the present study.

All of these parameters are related to the presence of fluids. Fault strength has an inverse relationship with pore pressure. The background seismicity rate can be presumed to reflect external forces (Hainzl & Ogata, 2005; Roland & McGuire, 2009; Llenos et al., 2009; Llenos & McGuire, 2011; Llenos & Michael, 2013), which include an increase in pore pressure. Stress drops and b-values are also reported to have an inverse and a direct relationship, respectively, with pore pressure (Wyss, 1973; Bachmann et al., 2011, 2012; Allmann and Shearer, 2007; Chen and Shearer, 2011; Goertz-Allmann et al., 2011). Moreover, intrinsic Q^{-1} is expected to increase with the presence of fluids (e.g., Winkler & Nur, 1982). Given that the obtained temporal variation in Q^{-1} reflects the change in intrinsic Q^{-1}, the observed temporal change can be also explained by the pore pressure change together with the temporal changes of other source and seismicity parameters. These synchronized temporal variations suggest that the pore pressure was high at the initial stage of this swarm and decreased with time and it affected the source- and seismicity- characteristics of the swarm.

The present swarm activity was estimated to have been triggered by a pore pressure increase after the 2011 Tohoku-Oki earthquake (Terakawa et al., 2013; Yoshida et al., 2016). In particular, the E-W extensional stress and the dynamic shaking caused by the Tohoku-Oki earthquake facilitated the ascent of fluids immediately below the source area of the swarm, generating a considerable pore pressure increase in the source area during the initial stage. The fluid diffusion indicated by the hypocenter migration in the swarm activity caused pore pressures to decrease over time. The obtained temporal pattern of Q^{-1} values, together with the patterns of fault strength, stress drop, background seismicity rate, and b-value, are consistent with this hypothesis.

While the attenuation is higher near earthquake sources than in the surrounding crust in the initial period of the swarm (<50 days after the 2011 Tohoku-Oki earthquake), they are not so different in the later periods (>50 days). The result suggests that the anelastic property in the source region of this swarm is not so different in a normal condition from the surrounding crust. In fact, seismicity level is quite low in this region before the 2011 Tohoku-Oki earthquakes, and this region did not seem special, except for the existence of an ancient caldera (Yoshida et al., 2016). An abrupt increase in pore pressure after the 2011 Tohoku-Oki earthquake, however, changed the condition, and caused a very intense earthquake swarm. Monitoring of Q^{-1} values at seismogenic depths would help to understand the states of potential seismogenic zones.

4 Discussion

4.1. Possibility of artificial temporal change in stress drop due to temporal change in near-source attenuation

Seismic waveform records from an earthquake supply information about the source, as well as the Earth’s structure. The correct separation of source- and propagation-effects is vital in order to examine the earthquake source and the structure. Two kinds of methods exist to extract information regarding the earthquake source: (1) empirical methods using waveforms of nearby earthquakes, such as Green’s function (EGF method; e.g., Hartzell, 1978) and (2) theoretical methods using simultaneously or independently estimated propagation- and site-effects, based on physical models (e.g., Andrew, 1986; Takahashi et al., 2005). One important factor for successfully separating the source effect is the possible existence of strong near-source attenuation. Ignoring this attenuation can lead to a systematic source-effect estimation error (e.g., Abercrombie, 2015).

The current study suggests that the intensity of seismic attenuation is higher near the earthquake sources than in the surrounding crust during the initial period of the swarm (< ~50 days after the Tohoku-Oki earthquake). Localized higher attenuation near the source leads to a systematic estimation error of the earthquake source effects; the attenuation is erroneously estimated as a part of the earthquake source signal.

Path- and site-effects are probably removed most effectively by EGF methods that use waveforms of nearby earthquakes as Green's function (hereafter a nearby event is referred to as an EGF event). However, even the results of EGF methods would be affected by ignoring near-source attenuation if the distance between the two events becomes larger. In fact, previous studies show that the source corner frequency determined using EGF methods is affected by the distance between the two events (Kane et al., 2013; Abercrombie, 2015). To avoid the effect of near-source attenuation, it is important to confirm that EGF events are sufficiently close to the target earthquake and/or to take the effect of near-source attenuation into account.

In the case of the Yamagata-Fukushima border swarm, average stress drop values of small earthquakes change with time almost synchronously with near-source attenuation. Although this may be explained by presuming that both parameters were affected by the temporal change in pore pressure, another possibility is that the temporal change in stress drop might be an artifact of the ignorance of changes in near-source attenuation.

However, it seems reasonable to consider that stress drops of small earthquakes actually changed with time after the 2011 Tohoku-Oki earthquakes in the source region of this swarm. Yoshida et al. (2017, 2019b) estimated stress drops for small earthquakes in this swarm using three different methods and obtained consistent results. Yoshida et al. (2017) first estimated frequency dependent Q^{-1} values and site-effects based on the coda normalization method (Aki, 1980; Philipps & Aki, 1986) and used the results for retrieving the source effects. Since they assumed that the Q^{-1} values are homogeneous both in space and time, the estimated source-effects in this approach might have been affected by the change in near-source attenuation. Yoshida et al. (2017) also estimated the stress drop based on the EGF method using S-coda waves, which effectively excludes the effects of near-source attenuation (Mayeda et al, 2007). Moreover, Yoshida et al. (2019b) estimated stress drops based on the EGF method using direct S-waves from very close earthquakes (< 0.5 km) as Green's functions, which is also not as susceptible to the effects of near-source attenuation, by taking rupture direction into account. Since all three results show similar temporal patterns of stress drops, it is reasonable to consider that the changes in stress drop are not an artifact. However, it is difficult to completely deny the possibility that the results are, to some extent, affected by the change in near-source attenuation over time.

4.2. Frequency-dependence of near-source attenuation

To evaluate the effects of near-source attenuation on source-effect estimation, knowledge of the frequency dependency of Q^{-1} is necessary. The near-source Q^{-1} values were estimated for the frequency ranges of 1-2 Hz and 4-8 Hz, in the same way as the results for 2-4 Hz (Fig. 5). The frequency distributions of Q^{-1} values are shown in Figs. 8 (a) and (b). The numbers are 1,071 and 1,932 for the frequency ranges of 1-2 Hz and 4-8 Hz, respectively. The median values are 0.028 (with a 95 % confidence interval of 0.024-0.032) and 0.009 (0.007-

0.010) for the frequency ranges of 1-2 Hz and 4-8 Hz, respectively. These values were also comparable to the regional value of ~0.01 for the source region estimated by Yoshida et al. (2017). Figs. 4 (b) and (c) show the frequency distributions of distance of earthquake-pairs used for the determination of Q^{-1} values. The median values are 1.1 - 1.2 km, similar among the three frequency ranges.

The Q^{-1} values obtained in this study tend to decrease with frequency as a whole: 0.028 in the 1-2 Hz frequency range, 0.011 in the 2-4 Hz, and 0.009 in the 4-8 Hz range, which is similar to the results of previous studies with frequency above 1Hz (Sato et al., 2012). The decreasing tendency of Q^{-1} with frequency also holds in the later period (Q^{-1}=0.025 for 1-2 Hz, 0.006 for 2-4 Hz, and 0.005 for 4-8 Hz). The decrease tendency of Q^{-1} with frequency suggests that the spectral shape and the corner frequency is not largely affected by the attenuation. Spectral amplitudes roughly become 90%, 95%, and 92% of the original amplitudes in the frequency range of 1-2 Hz, 2-4 Hz, and 4-8 Hz, respectively, by the attenuation structure after propagating 3 km (t=0.9s) near the source based on Eq. (1). However, Q^{-1} does not clearly decrease with frequency in the initial period (Q^{-1}=0.035 for 1-2 Hz, 0.040 for 2-4 Hz, and 0.031 for 4-8 Hz), which affects the spectral shape. Spectral amplitudes roughly become 86%, 71%, and 60% of the original amplitudes in the frequency range of 1-2 Hz, 2-4 Hz, and 4-8 Hz, respectively, after propagating 3 km.

The temporal changes of the median values are shown in Fig. 8 (e) and (f), in which the median values were computed from each bin that had 50 results ordered by time. Although individual values are scattered, the median values change with time similar to the results from the 2-4 Hz frequency range (Fig. 5b). The temporal changes are consistent with the hypothesis that the temporal change in pore pressure affects the anelastic property in the source region of the present swarm. However, the decay patterns seem different among the three frequency ranges. In particular, Q^{-1} of 1-2 Hz decrease with time more gradually than those of 2-4 Hz and 4-8 Hz. It is difficult to exactly know the cause of the different temporal pattern and the complex frequency dependence of Q^{-1}. They might include information about the state of fluids such as the spatial extent of pores.

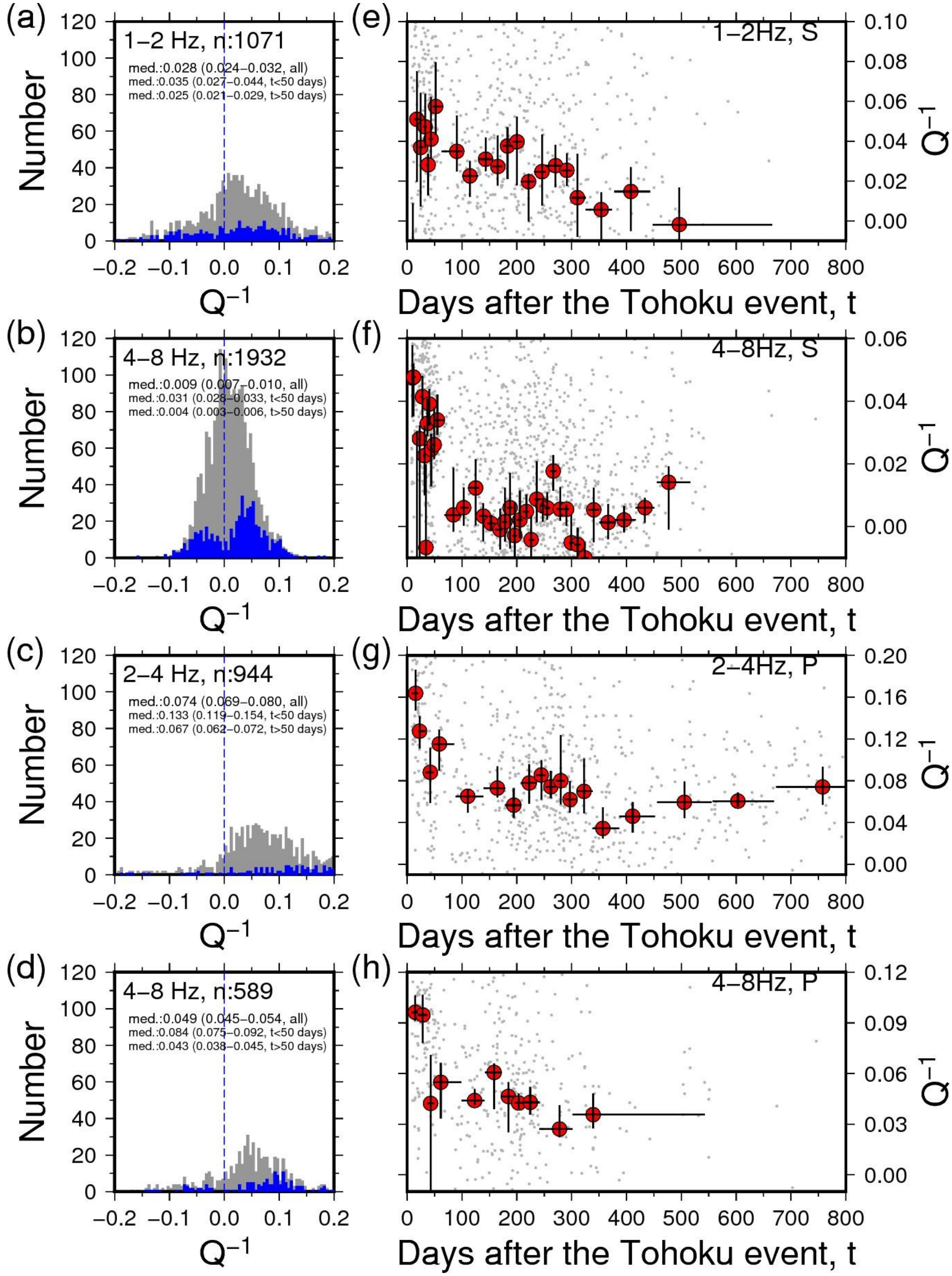
(a)
1–2 Hz, n:1071
med.:0.028 (0.024–0.032, all)
med.:0.035 (0.027–0.044, t<50 days)
med.:0.025 (0.021–0.029, t>50 days)
(b)
4–8 Hz, n:1932
med.:0.009 (0.007–0.010, all)
med.:0.031 (0.028–0.033, t<50 days)
med.:0.004 (0.003–0.006, t>50 days)
(c)
2–4 Hz, n:944
med.:0.074 (0.069–0.080, all)
med.:0.133 (0.119–0.154, t<50 days)
med.:0.067 (0.062–0.072, t>50 days)
(d)
4–8 Hz, n:589
med.:0.049 (0.045–0.054, all)
med.:0.084 (0.075–0.092, t<50 days)
med.:0.043 (0.038–0.045, t>50 days)
Number
Q−1
(e)
1–2Hz, S
(f)
4–8Hz, S
(g)
2–4Hz, P
(h)
4–8Hz, P
Days after the Tohoku event, t

Figure 8. Results of near-source attenuation. (a)-(d): Frequency distribution of obtained near-source Q^{-1}-values. (e)-(h): Temporal change in near-source Q^{-1}-values. (a), (e): Results for the frequency ranges of 1-2 Hz from S-waves. (b), (f): Results for the frequency ranges of 4-8 Hz from S-waves. (c), (g): Results for the frequency ranges of 2-4 Hz from P-waves. (d), (h): Results for the frequency ranges of 4-8 Hz from P-waves. Other details are the same as in Fig. 5.

4.3. Near-source attenuation of P-wave

The Q^{-1} values of P-waves were also estimated using the same procedure as that of the S-waves, but used the vertical component of the waveforms. These results are shown in Fig. 8 (c) and (d) by their frequency distributions. Since the S/N ratios were very small in the 1-2 Hz frequency range, only the results for the 2-4 Hz and 4-8 Hz frequency ranges are shown. The values are 994 and 589 for the 2-4 Hz and 4-8 Hz frequency ranges, respectively. The median values are 0.074 (with a 95 % confidence interval of 0.069-0.080) and 0.049 (0.045-0.054) for the 2-4 Hz and 4-8 Hz frequency ranges, respectively. The values tend to be higher than those estimated using S-waves. This is the opposite of what is expected, based on theoretical considerations in a simple model (Knopoff, 1971), but is consistent with the results obtained by Hauksson & Shearer (2006) for the southern California crust. As suggested by Hauksson & Shearer (2006), this can probably be explained by including the contribution of crustal pore fluids to the attenuation of seismic waves. The temporal changes of the median values at each bin having 50 results are shown in Fig. 8 (g) and (h). The median values change with time similar to the results from S-wave.

4.4. Effects of the radiation pattern difference on the estimation of near-source attenuation

The present study utilized nearby earthquake pairs with similar focal mechanisms to estimate the attenuation parameter near the sources. In the previous sections, it was assumed that the difference of radiation patterns of the two events is small enough not to affect the determination of Q^{-1}-value. In this subsection, I examined the effects of the radiation-pattern difference on the temporal change in near-source Q^{-1}- value.

I used synthetic amplitude ratios of earthquake-pairs to evaluate the effects of radiation-pattern difference. I computed synthetic amplitude ratios of S-waves for earthquake-pairs used for the determination of Q^{-1}- values based on the equation of Dahm (1996) by using moment tensors determined by Yoshida et al. (2019). Synthetic amplitude ratios were computed at each seismic station used for the measurement of Q^{-1}-value. I then applied the same method used in this study for determining Q^{-1}-value to synthetic amplitude ratio data with actual differential arrival time data.

The frequency distribution of near-source Q^{-1} thus synthetically produced is shown in Fig. 9 (a). The median value is 0.000 and the 95 % confidence region is from -0.001 to 0.001. Unlike the results of real data, the number of negative Q^{-1}-value (n: 937) is almost comparable to that of positive Q^{-1}-value (n: 947). This indicates that effects of radiation pattern difference do not bias the estimates of Q^{-1}-value. Moreover, the median values of Q^{-1} do not significantly change between the initial period (the 95 % frequency range is from -0.003 to 0.003) and the later period (the 95 % frequency range is from -0.001 to 0.001). The synthetic results does not show a decreasing tendency of Q^{-1} with time (Fig. 9b) as obtained for real data (Fig. 5b). This indicates that effects of the difference of radiation pattern cannot explain the observed temporal variation of Q^{-1}-value.

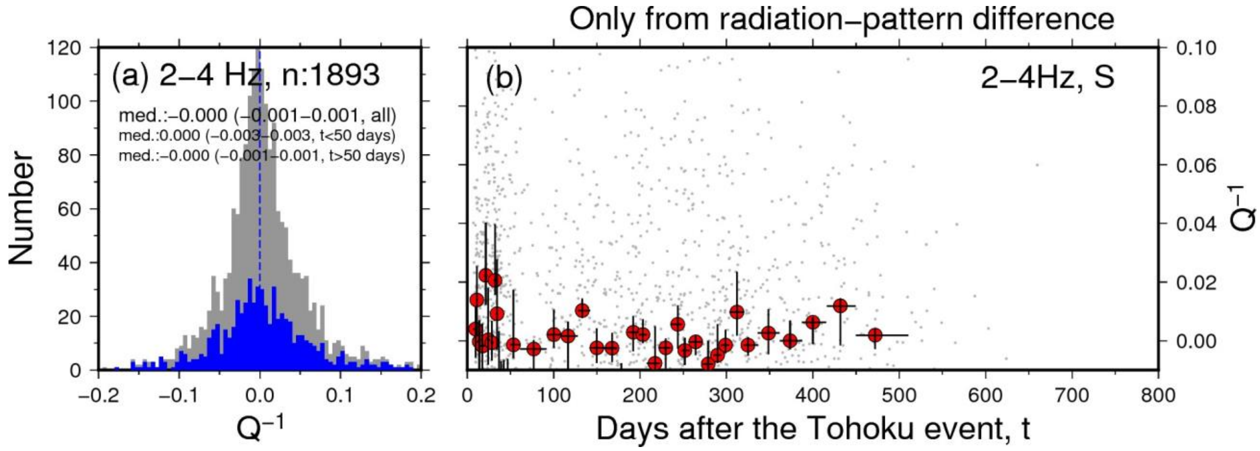

Figure 9. Results of the synthetic test of near-source attenuation analyses. (a) Frequency distribution of obtained near-source Q^{-1}-values. Gray shows the result for all the analyzed periods. Blue shows the results for up to 50 days after the 2011 Tohoku-Oki earthquake. (b) Temporal changes in the near-source Q^{-1}-values. Gray circles show individual results and red circles show median values of 20 bins having the same number of results. Vertical line indicates the 95% confidential interval based on 2000 bootstrap re-samplings.

5 Conclusions

This study examined the near-source attenuation in the focal region of the intense swarm activity in the Yamagata-Fukushima border region of Japan, which was estimated to have been triggered by fluid movement after the 2011 Tohoku-Oki earthquake (Terakawa et al., 2013; Yoshida et al., 2016). Near-source attenuation was estimated based on a new technique that precisely examines the decay of the amplitude ratios of two nearby earthquakes with travel time differences by using similar waveforms. The obtained Q^{-1} values vary over a wide range, but their median values exhibit a characteristic temporal variation: Q^{-1} is large for the initial ~50 days (with a median value of 0.041), and significantly decreased to become almost constant after 50 days (with a median value of 0.006) for S-wave of the frequency range of 2-4 Hz. The same tendency was obtained for all analyzed frequency ranges of both P- (2-4, 4-8 Hz) and S-waves (1-2, 2-4, 4-8 Hz). These temporal patterns are similar to those independently obtained for background seismicity rates, b-values, stress drops, and fault strength. The synchronous change supports the hypothesis that the swarm was triggered by fluid movement after the 2011 Tohoku-Oki earthquake, and that the source and seismicity characteristics were affected by temporal changes in fault strength affected by pore pressure.

This study suggests the possibility that the seismic attenuation intensity is higher near the earthquake sources than in the surrounding crust in some situations. Localized higher attenuation near the source leads to a systematic estimation error of earthquake source effects; the attenuation is erroneously estimated as a part of the earthquake source signal. It is therefore important to examine the intensity and the frequency dependence of near-source attenuation to accurately estimate earthquake source properties.

The method used in the current study cannot handle frequency ranges higher than the source corner frequency. In fact, it is necessary to understand the attenuation behavior at such frequencies (> 8 Hz), because it is closely related to estimating source-effects for small earthquakes. The estimation of near-source attenuation at higher frequency ranges would be possible in a future study by analyzing the waveform data from smaller earthquakes (M<2) using dense temporary seismic network data.

Acknowledgments and Data

This study used hypocenters and P-and S-wave arrival time data reported in the unified catalogue of the Japan Meteorological Agency. The seismograms were collected and stored by JMA, national Universities, and NIED (http://www.hinet.bosai.go.jp/?LANG=en). The figures were created using GMT (Wessel and Smith, 1998). The comments from Genti Toyokuni on the first draft significantly improved the manuscript. Obtained results of Q^{-1} are available at http://www.aob.gp.tohoku.ac.jp/~yoshida/pub/JGR2019/.

References

Abercrombie, R. E. (2015). Investigating uncertainities in empirical Green's function analysis of earthquake source parameters. *Journal of Geophysical Research-Solid Earth*, 4263–4277. https://doi.org/10.1002/2015JB011984.

Aki, K. (1967). Scaling law of seismic spectrum. Journal of Geophysical Research, 72(4), 1217–1231.

Aki, K. (1980). Attenuation of shear-waves in the lithosphere for frequencies from 0.05 to 25 Hz. *Physics of the Earth and Planetary Interiors*, *21*(1), 50–60.

Andrews, D. J. (1986). Objective determination of source parameters and similarity of earthquakes of different size. *Earthquake Source Mechanics*, *37*, 259–267.

Bachmann, C. E., Wiemer, S., Woessner, J., & Hainzl, S. (2011). Statistical analysis of the induced Basel 2006 earthquake sequence: Introducing a probability-based monitoring approach for Enhanced Geothermal Systems. *Geophysical Journal International*, *186*(2), 793–807. https://doi.org/10.1111/j.1365-246X.2011.05068.x

Chen, X., & Shearer, P. M. (2011). Comprehensive analysis of earthquake source spectra and swarms in the Salton Trough, California. *Journal of Geophysical Research: Solid Earth*, *116*(9), 1–17. https://doi.org/10.1029/2011JB008263

Dahm, T. (1996). Relative moment tensor inversion based on ray theory: theory and synthetic tests. Geophysical Journal International, 124(1), 245–257.

Goertz-Allmann, B. P., Goertz, A., & Wiemer, S. (2011). Stress drop variations of induced earthquakes at the Basel geothermal site. *Geophysical Research Letters*, *38*(9), https://doi.org/10.1029/2011GL047498

Hainzl, S., & Ogata, Y. (2005). Detecting fluid signals in seismicity data through statistical earthquake modeling. *Journal of Geophysical Research: Solid Earth*, *110*(5), 1–10. https://doi.org/10.1029/2004JB003247

Hartzell, S. H. (1978). Earthquakes aftershocks as Green's Functions. *Geophysical Research Letters*, *5*(1), 1–4. https://doi.org/10.1029/GL005i001p00001

Hasegawa, A., Nakajima, J., Umino, N., & Miura, S. (2005). Deep structure of the northeastern Japan arc and its implications for crustal deformation and shallow seismic activity. *Tectonophysics*, *403*(1–4), 59–75. https://doi.org/10.1016/j.tecto.2005.03.018

Hauksson, E., & Shearer, P. M. (2006). Attenuation models (QP and QS) in three dimensions of the southern California crust: Inferred fluid saturation at seismogenic depths. *Journal of Geophysical Research: Solid Earth*, *111*(B5).

Hubbert, M. K., & Rubey, W. W. (1959). Role of fluid overpressure in the mechanics of overthrust faulting. *Geological Society of America Bulletin*, *70*, 167–206. https://doi.org/10.1130/0016-7606(1959)70

Kane, D. L., Kilb, D. L., & Vernon, F. L. (2013). Selecting empirical Green's functions in regions of fault complexity: A study of data from the San Jacinto fault zone, southern California. *Bulletin of the Seismological Society of America*, *103*(2A), 641–650.

Kaneko, Y., & Shearer, P. M. (2014). Seismic source spectra and estimated stress drop derived from cohesive-zone models of circular subshear rupture. Geophysical Journal International, 197(2), 1002–1015. https://doi.org/10.1093/gji/ggu030

Knopoff, L. (1971). Attenuation, in mantle and core in planetary physics. Elsevier.

Kriegerowski, M., Cesca, S., Ohrnberger, M., Dahm, T., & Krüger, F. (2019). Event couple spectral ratio Q method for earthquake clusters: application to northwest Bohemia. *Solid Earth*, *10*(1), 317–328.

Llenos, A. L., McGuire, J. J., & Ogata, Y. (2009). Modeling seismic swarms triggered by aseismic transients. *Earth and Planetary Science Letters*, *281*(1–2), 59–69. https://doi.org/10.1016/j.epsl.2009.02.011

Llenos, A. L., & Michael, A. J. (2013). Modeling earthquake rate changes in Oklahoma and Arkansas: Possible Signatures of induced seismicity. *Bulletin of the Seismological Society of America*, *103*(5), 2850–2861. https://doi.org/10.1785/0120130017

Matsumoto, S., Uehira, K., Watanabe, A., Goto, K., Iio, Y., Hirata, N., … others. (2009). High resolution Q- 1 estimation based on extension of coda normalization method and its application to P-wave attenuation structure in the aftershock area of the 2005 West Off Fukuoka Prefecture Earthquake (M 7.0). *Geophysical Journal International*, *179*(2), 1039–1054.

Mayeda, K., Malagnini, L., & Walter, W. R. (2007). A new spectral ratio method using narrow band coda envelopes: Evidence for non-self-similarity in the Hector Mine sequence. *Geophysical Research Letters*, *34*(11), 2–6. https://doi.org/10.1029/2007GL030041

Nur, A., & Booker, J. R. (1972). Aftershocks caused by pore fluid flow? *Science*, *175*(4024), 885–887. https://doi.org/10.1126/science.175.4024.885

Okada, T., Matsuzawa, T., Umino, N., Yoshida, K., Hasegawa, A., Takahashi, H., … Miyamachi, H. (2016). Hypocenter migration and crustal seismic velocity distribution observed for the inland earthquake swarms induced by the 2011 Tohoku-Oki earthquake in NE Japan: Implications for crustal fluid distribution and crustal permeability. In *Crustal Permeability*. https://doi.org/10.1002/9781119166573.ch24

Phillips, W. S., & Aki, K. (1986). Site amplification of coda waves from local earthquakes in central California. *Bulletin of the Seismological Society of America*, *76*(3), 627–648.

Roland, E., & McGuire, J. J. (2009). Earthquake swarms on transform faults. *Geophysical Journal International*, *178*(3), 1677–1690. https://doi.org/10.1111/j.1365-246X.2009.04214.x

Sato, H., Fehler, M. C., & Maeda, T. (2012). *Seismic wave propagation and scattering in the heterogeneous earth* (Vol. 496). Springer.

Shapiro, S. A., Huenges, E., & Borm, G. (1997). Estimating the crust permeability from fluid-injection-induced seismic emission at the KTB site. *Geophysical Journal International*, *131*(2). https://doi.org/10.1111/j.1365-246X.1997.tb01215.x

Shelly, D. R., Ellsworth, W. L., & Hill, D. P. (2016). Fluid-faulting evolution in high definition: Connecting fault structure and frequency-magnitude variations during the 2014 Long Valley Caldera, California, earthquake swarm. *Journal of Geophysical Research: Solid Earth*, *121*(3), 1776–1795. https://doi.org/10.1002/2015JB012719

Sibson, R. H. (1992). Implications of fault-valve behaviour for rupture nucleation and recurrence. *Tectonophysics*, *211*(1–4), 283–293. https://doi.org/10.1016/0040-1951(92)90065-E

Terakawa, T., Hashimoto, C., & Matsu'ura, M. (2013). Changes in seismic activity following the 2011 Tohoku-oki earthquake: Effects of pore fluid pressure. *Earth and Planetary Science Letters*, *365*, 17–24. https://doi.org/10.1016/j.epsl.2013.01.017

Ueno, H., Hatakeyama, S., Aketagawa, T., Funasaki, J., & Hamada, N. (2002). Improvement of hypocenter determination procedures in the Japan Meteorological Agency. *Q. J. Seismol.*, *65*, 123–134.

Wessel, P., & Smith, W. H. F. (1998). New, improved version of generic mapping tools released. *Eos, Transactions American Geophysical Union*, *79*(47), 579–579. https://doi.org/10.1029/98EO00426

Winkler, K. W., & Nur, A. (1982). Seismic attenuation: Effects of pore fluids and frictional-sliding. Geophysics, 47(1), 1–15.

Wyss, M. (1973). Towards a Physical Understanding of the Earthquake Frequency Distribution. *Geophysical Journal of the Royal Astronomical Society*, *31*(4), 341–359. https://doi.org/10.1111/j.1365-246X.1973.tb06506.x

Yoshida, K., & Hasegawa, A. (2018). Hypocenter Migration and Seismicity Pattern Change in the Yamagata-Fukushima Border, NE Japan, Caused by Fluid Movement and Pore Pressure Variation. *Journal of Geophysical Research: Solid Earth*, *123*(6), 5000–5017. https://doi.org/10.1029/2018JB015468

Yoshida, K., Hasegawa, A., Yoshida, T., & Matsuzawa, T. (2019a). Heterogeneities in stress and strength in tohoku and its relationship with earthquake sequences triggered by the 2011 M9 Tohoku-Oki earthquake. *Pure and Applied Geophysics*, *176*(3), 1335–1355.

Yoshida, K., Saito, T., Emoto, K., Urata, Y., & Sato3, D. (2019b). Rupture directivity, stress drop, and hypocenter migration of small- and moderate-sized earthquakes in the Yamagata-Fukushima border swarm triggered by upward pore-pressure migration after the 2011 Tohoku-Oki earthquake. *Tectonophysics*.

Yoshida, K., Saito, T., Urata, Y., Asano, Y., & Hasegawa, A. (2017). Temporal Changes in Stress Drop, Frictional Strength, and Earthquake Size Distribution in the 2011 Yamagata-Fukushima, NE Japan, Earthquake Swarm, Caused by Fluid Migration. *Journal of Geophysical Research: Solid Earth*, *122*(12), 10,379-10,397. https://doi.org/10.1002/2017JB014334

Yoshida, K., Hasegawa, A., & Yoshida, T. (2016). Temporal variation of frictional strength in an earthquake swarm in NE Japan caused by fluid migration. *Journal of Geophysical Research: Solid Earth*, *121*(8), 5953–5965. https://doi.org/10.1002/2016JB013022